European Journal of Immunology

Nitric oxide inhibits the accumulation of $CD4^+CD44^{hi}Tbet^+CD69^{lo}$ T cells in mycobacterial infection

John E. Pearl[*1], Egidio Torrado*[*1], Michael Tighe[1], Jeffrey J. Fountain[1], Alejandra Solache[1,2], Tara Strutt[4], Susan Swain[4], Rui Appelberg[3] and Andrea M. Cooper[1]*

[1] Trudeau Institute Inc., Saranac Lake, NY, USA
[2] Millipore, Temecula, CA, USA
[3] Instituto de Biologia Molecular e Celular (IBMC), University of Porto, Portugal
[4] Department of Pathology, University of Massachusetts Medical School, Worcester, MA, USA

Animals lacking the inducible nitric oxide synthase gene (*nos2*$^{-/-}$) are less susceptible to *Mycobacterium avium* strain 25291 and lack nitric oxide-mediated immunomodulation of $CD4^+$ T cells. Here we show that the absence of *nos2* results in increased accumulation of neutrophils and both $CD4^+$ and $CD8^+$ T cells within the *M. avium* containing granuloma. Examination of the T-cell phenotype in *M. avium* infected mice demonstrated that $CD4^+CD44^{hi}$ effector T cells expressing the Th1 transcriptional regulator T-bet ($T\text{-}bet^+$) were specifically reduced by the presence of nitric oxide. Importantly, the $T\text{-}bet^+$ effector population could be separated into $CD69^{hi}$ and $CD69^{lo}$ populations, with the $CD69^{lo}$ population only able to accumulate during chronic infection within infected *nos2*$^{-/-}$ mice. Transcriptomic comparison between $CD4^+CD44^{hi}CD69^{hi}$ and $CD4^+CD44^{hi}CD69^{lo}$ populations revealed that $CD4^+CD44^{hi}CD69^{lo}$ cells had higher expression of the integrin *itgb1/itga4* (VLA-4, CD49d/CD29). Inhibition of Nos2 activity allowed increased accumulation of the $CD4^+CD44^{hi}T\text{-}bet^+CD69^{lo}$ population in WT mice as well as increased expression of VLA-4. These data support the hypothesis that effector T cells in mycobacterial granulomata are not a uniform effector population but exist in distinct subsets with differential susceptibility to the regulatory effects of nitric oxide.

Keywords: Bacterial infection · $CD4^+$ T cells · Cell differentiation · Immunopathology · Inflammation

Supporting Information available online

Introduction

Infection with *Mycobacterium* species can result in chronic disease and sustained stimulation of the immune response that needs to be regulated in order to control bacterial growth without destroying host tissue [1]. Nitric oxide has a wide variety of regulatory activities, which can affect the chronic host response to infection [2–5]. In the case of *Mycobacterium avium,* the bacteria are not susceptible to the toxic effects of nitric oxide [6], allowing us to probe the role of reactive nitrogen intermediates

Correspondence: Dr. Andrea M. Cooper
e-mail: acooper@trudeauinstitute.org

*These authors contributed equally to this work.

in regulation of the T-cell response to mycobacterial infection without the confounding factor of uncontrolled bacterial growth.

Nitric oxide acts on physiological systems with effects dependent upon concentration, the relative levels of reactive oxygen radicals and pH [7]. At low concentrations, nitric oxide acts as a signaling molecule, either in a cGMP-dependent or -independent manner, to promote vascular integrity, mediate neurotransmission, and regulate cellular respiration by altering the affinity of cytochrome C for oxygen [7, 8]. At high concentrations, nitric oxide inhibits respiration and causes nitrosative damage to proteins, lipid peroxidation, and DNA [9, 10]. The balance between nitric oxide and oxygen radicals is important, as nitric oxide can reduce oxidative stress [11] but also generates peroxynitrite, which is itself damaging [12]. The damage generated by high levels of nitric oxide is detrimental to cells and results in apoptosis [9].

The impact of nitric oxide on the immune response has been extensively analyzed with identification of both positive and negative regulatory roles [13]. In humans, nitric oxide limits IL-2 release and proliferation of T cells via activation of the cGMP-dependent protein kinase, cGK I [14]. In *Trypanosoma brucei* mouse models, nitric oxide inhibits the accumulation of IL-2- and IFN-γ-producing T cells [15]. In both an in vitro system [16] and a *Listeria monocytogenes* mouse model [17], the inhibition of nitric oxide synthase (Nos) results in improved antigen-specific T-cell responses. Nitric oxide also acts as an anti-inflammatory agent by limiting the interaction of leucocytes with the endothelial monolayer [18]. Nitric oxide can drive IL-10-producing regulatory T cells, limit the expansion of Th17 cells [19, 20], and regulate the IL-12 pathway both positively [21] and negatively [22]. Indeed, at low levels, it can augment the generation of Th1 cells by increasing expression of IL-12Rβ2 [23, 24] and augment IFN-γ—mediated signaling [25].

In mycobacterial disease, nitric oxide is essential for the control of *Mycobacterium tuberculosis* but dispensable for the control of *M. avium* [4]. It limits the accumulation of activated T cells in the *Mycobacterium bovis* BCG model [26], the *M. tuberculosis* model [27], and the *M. avium* model [6] with an increased IFN-γ response being seen in both *M. avium* [6] and *M. tuberculosis* infected *nos2*$^{-/-}$ mice [28]. Absence of nitric oxide in *M. avium* infection results in lesions with increased cellularity and collagen deposition [6, 29, 30]. Thus, nitric oxide acts to limit T-cell responses and immunopathology during mycobacterial infection and in the absence of nitric oxide, there is improved IFN-γ production [6].

The impact of nitric oxide on specific subsets of activated T cells has not been extensively studied; however, recent data shows that while some antigen-specific CD4$^+$ T-cell effectors are able to persist within the mycobacterially induced inflammatory environment, other effector cells are not [31]. Specifically, T cells that can produce IFN-γ but which maintain the capacity to proliferate are better able to persist in mycobacterially infected mice than are T cells with higher IFN-γ production but lower proliferative capacity [31]. As nitric oxide is known to be involved in both initiation and regulation of the IFN-γ-producing CD4$^+$ T-cell population, we investigated whether different subsets of effector CD4$^+$ T cells were differentially susceptible to nitric oxide during mycobacterial disease.

Results

The bacterial burden and the granuloma in WT and *nos2*$^{-/-}$ mice differ

We examined bacterial burden and granuloma formation following a moderate intravenous dose of *M. avium* 25291. Figure 1A demonstrates that growth of *M. avium* 25291 was reduced in *nos2*$^{-/-}$ mice compared with that in wild-type (WT) mice and that cellular inflammation was different between the two groups [30, 32]. There was a preponderance of mononuclear phagocytes with large cytoplasm in the WT mice (Fig. 1B) while the lesions in the *nos2*$^{-/-}$ mice were more circumscribed with macrophages and lymphocytes forming a mantle around a central area of neutrophil-like cells (Fig. 1C). These data confirm that the WT and *nos2*$^{-/-}$ mice differ in response to *M. avium* 25291 with impaired bacterial control in WT mice and more complex granuloma development in the *nos2*$^{-/-}$ mice.

Absence of Nos2 promotes lymphocytes and granulocytes accumulation in the *M. avium* induced lesion

To better define the cells within the WT and *nos2*$^{-/-}$ lesions, we probed live sections of infected liver tissue with antibody specific for macrophage (F4/80), neutrophil (Ly6G), and lymphocyte (CD4 and CD8) markers.

We found greater numbers of CD4$^+$ or CD8$^+$ cells throughout the F4/80$^+$ macrophage defined lesion in the *nos2*$^{-/-}$ mouse (Fig. 2B) compared with the WT mouse (Fig. 2A). Further, there were significantly more Ly6G$^+$ cells within the *nos2*$^{-/-}$ lesions (Fig. 2D) compared to the WT lesions (Fig. 2C) and these appeared to coalesce in central areas (Fig. 2D). These data show that both lymphocytes and neutrophils accumulate more readily within the macrophage-defined lesions of *M. avium* infected *nos2*$^{-/-}$ compared to WT mice.

As lymphocytes were absent from the WT lesions, we wanted to compare the environment created within the F4/80 dominated lesions of the WT and *nos2*$^{-/-}$ mice. To do this, we stained cryosections from infected WT and *nos2*$^{-/-}$ livers for the enzymes required to generate toxic oxygen and nitrogen radicals. We found that p22-phox, a critical subunit of the NADPH oxidase required for oxygen radical generation [33], was readily expressed throughout the phagocyte areas of both WT (Fig. 2E) and *nos2*$^{-/-}$ mice (Fig. 2F). The Nos2 protein was less widely expressed in the WT lesions (Fig. 2G)

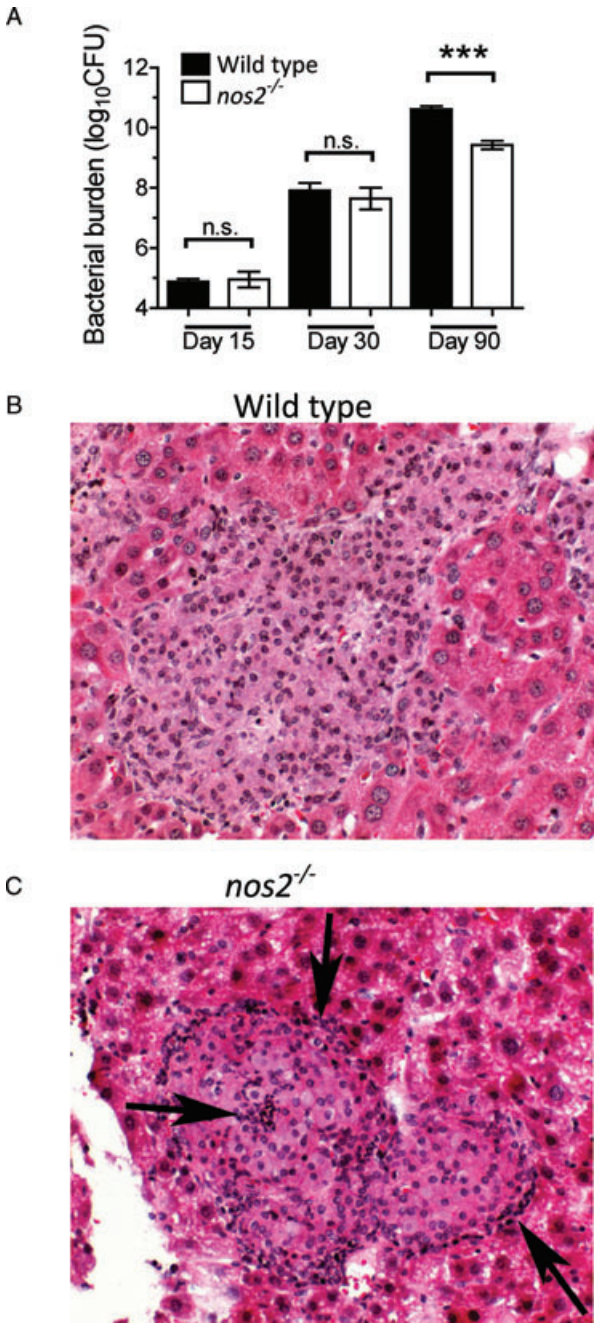

Figure 1. Bacterial burden and inflammation differ in *Mycobacterium avium* infected WT and *nos2*$^{-/-}$ mice. (A) WT (black bars) and *nos2*$^{-/-}$ (white bars) mice were infected intravenously with 10^6 *M. avium* 25291, livers were harvested on the indicated days and the number of colony forming units determined. Data are shown as mean + SEM of $n = 5$ and are representative of three independent experiments. $^{***}p < 0.001$, Student's *t*-test. (B, C) Livers from infected (B) WT and (C) *nos2*$^{-/-}$ mice were also processed for histological analysis on day 120 using hematoxylin and eosin (original magnification 200×). Arrows in (C) show margin of granuloma and central area of granulocytic cells not present in (B). Data shown are representative of five animals per group and two similar experiments.

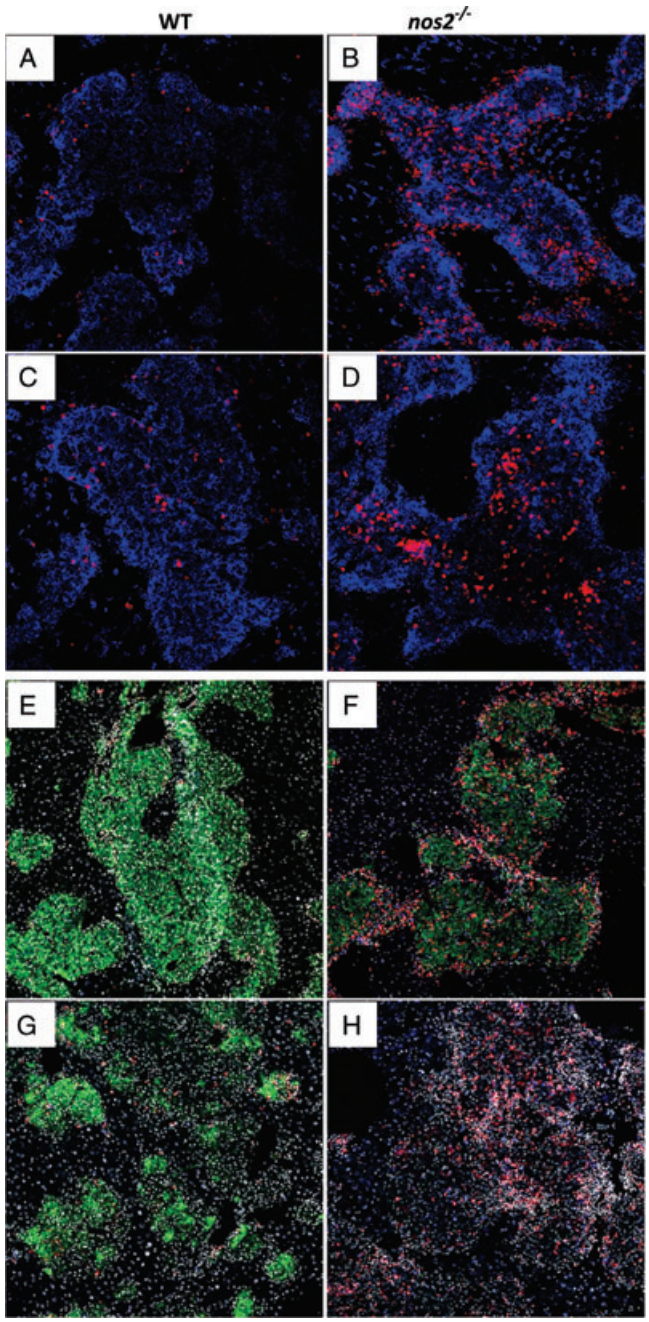

Figure 2. The absence of Nos2 promotes accumulation of lymphocytes and granulocytes in the *Mycobacterium avium* induced lesion. WT (A, C, E, G) and *nos2*$^{-/-}$ (B, D, F, H) mice were infected intravenously with 10^6 *M. avium* 25291 and the livers harvested on day 120. (A–D) Livers were placed directly in agar and rapidly sectioned without fixation using a vibrating microtome. Tissue slices were stained with the F4/80 antibody (blue in A–D) and anti-CD4/CD8 antibody (red in A and B) or anti-Ly6G antibody (red in C and D, original magnification 200×). Data shown are representative of six total animals over three experiments. (E–H) Livers were also harvested for cryosectioning and frozen sections were stained for CD4 (red) CD8 (blue) and either p22-phox (green, E, F) or Nos2 (green G, H, original magnification 200×). Nuclear stain is white. Data shown are representative of four animals per group, and of two experiments performed.

and was absent in the *nos2*$^{-/-}$ lesions (Fig. 2H). Both CD4$^+$ (red) and CD8$^+$ (blue) cells were seen in the p22-phox positive WT tissues (Fig. 2E) but were much more prevalent in the p22-phox area in the *nos2*$^{-/-}$ tissues (Fig. 2F). The CD4$^+$ T cells were significantly increased in the sections from *nos2*$^{-/-}$ livers with an average of $321^{\pm 100}$ CD4$^+$ cells per section versus an average of $93^{\pm}29$ cells per section in the WT ($p = 0.0046$ by Student's *t*-test). These data demonstrate that while Nos2 is not as widely expressed as p22-phox, it severely affects the ability of CD4$^+$ and CD8$^+$ lymphocytes to accumulate within the mycobacterial granuloma.

Activated effector lymphocytes within infected organs are differentially affected by nitric oxide

Mycobacterium avium infected WT mice undergo a profound IFN-γ-dependent depletion of lymphocytes; however, the impact of Nos2 in this model is not to substantially deplete T cells but to reduce the level of the IFN-γ response [6, 34]. Figure 2 suggests that T cells are specifically excluded from the phagocytic areas in *M. avium* infected WT mice in a nitric oxide-dependent manner. To determine whether the histological results in the WT lesions represented the depletion of all or a specific subset of lymphocytes from the affected organ, we compared the CD4$^+$ T cells within infected organs by flow cytometry. We found only a modest effect of *nos2* deficiency on the total frequency and number of either live lymphocytes or CD4$^+$ T cells in infected organs compared to WT mice (Supporting Information Fig. 1). This trend was seen before but had not reached statistical significance in previous studies [6, 34].

To determine whether the *nos2* gene was adversely affecting activated effector cells, we compared the frequency (Fig. 3A) and number (Fig. 3B) of CD4$^+$ T cells expressing the Th1-associated transcription factor, T-bet. We found that the CD4$^+$ T-bet$^+$ population was significantly and substantially increased in the *nos2*$^{-/-}$ mice relative to the WT mice in all infected organs (Fig. 3). These data demonstrate that the presence of *nos2* limits the accumulation of Th1-type T cells and that these activated effector cells were either more susceptible to depletion or failed to develop in the presence of Nos2.

To investigate whether all activated T-bet$^+$ cells were equally affected by the presence of *nos2,* we stained CD4$^+$ T cells from all infected organs for both T-bet and CD69, a molecule that is upregulated upon antigen exposure [35]. The pattern of staining is shown in Fig. 4A. We found that in all three organs, the frequency and number (Fig. 4B) of CD69^{hi} T-bet$^+$ CD4$^+$ T cells were only modestly affected by the absence of *nos2*. In contrast, the CD69^{lo}T-bet$^+$ CD4$^+$ T-cell population failed to accumulate in the WT mice but did accumulate in the spleen, liver, and lung of the *nos2*$^{-/-}$ mice (Fig. 4C). These data demonstrate that the *nos2* gene has the capacity to limit accumulation of CD69^{lo}T-bet$^+$ CD4$^+$ T cells.

CD4$^+$CD44^{hi}CD69^{hi} and CD4$^+$CD44^{hi}CD69^{lo} cells have distinct transcriptomes in vivo

To define the basis of the increased susceptibility to *nos2* of the CD69^{lo}T-bet$^+$ cells relative to the CD69^{hi}T-bet$^+$ cells, we compared gene transcription immediately ex vivo in CD4$^+$ T cells sorted based on CD44 and CD69 expression using an unbiased microarray approach. Equivalent numbers of cells differing only in the expression of CD69 (CD4$^+$CD44^{hi}CD69^{hi} versus CD4$^+$CD44^{hi}CD69^{lo}), were purified using fluorescence-activated cell sorting from the splenocytes of WT and *nos2*$^{-/-}$ mice infected with *M. avium* 80 days previously (all CD44^{hi} cells are T-bet$^+$ in this model, data not shown). Global RNA expression was analyzed for differential gene expression and class comparison (Fig. 5). We found that there was differential expression between the four populations of cells of 911 sequences detected by unique probes and that the patterns for individual mice within each group were reproducible (Fig. 5A). Importantly, we found that gene expression patterns were associated with both genotype of the mouse (WT versus *nos2*$^{-/-}$) and phenotype of the cells (CD69^{hi} versus CD69^{lo}) and that there were differences between the gene expression patterns for the CD4$^+$CD44^{hi}CD69^{lo} cells isolated from WT and *nos2*$^{-/-}$ mice (black arrows in Fig. 5A). The log intensity values of the microarray data set are available in Supporting Information Table 1.

To probe the data sets for biological relevance, we compared the differential gene expression data against 218 predefined gene lists representing previously investigated mouse biological processes. Two pathways were identified as being significantly represented in the differentially expressed data set and both contained the genes for the heterodimeric integrin known as very late antigen-4 (VLA-4, CD49d/CD29) (Fig. 5B).

By further comparing specific gene expression within the individual samples ($n = 3$), we were able to define statistically different gene expression for genes of interest. We found that the CD4$^+$CD44^{hi}CD69^{lo} population from both the WT and *nos2*$^{-/-}$ infected mice expressed less *il2*, *il2ra*, *il2rb,* and *ifngr2* than did the CD4$^+$CD44^{hi}CD69^{hi} population (Table 1). By comparing the expression of genes between cell subsets from the WT and *nos2*$^{-/-}$ mice, we found that *bcl2* expression was reduced in the absence of nitric oxide for both of the types of cells (Table 1). However, only within the CD4$^+$CD44^{hi}CD69^{lo} population was there an impact of nitric oxide on the expression of *il4* and to a lesser degree on *il4ra* (Table 1). Interestingly, there is no difference in the expression of the *tbx21* (T-bet) or *gata3* master regulators for IFN-γ and IL-4 within these populations (data not shown). Taken together, the data support the fact that the activated effector cells within the mycobacterial granuloma can be grouped into potentially functional subsets by surface markers. In particular, the CD4$^+$CD44^{hi}CD69^{hi} population may represent an IL-2-producing and IL-2- and IFN-γ-responsive, potentially proliferating population whereas the CD4$^+$CD44^{hi}CD69^{lo} may be unresponsive to IL-2 and IFN-γ. The strong need for

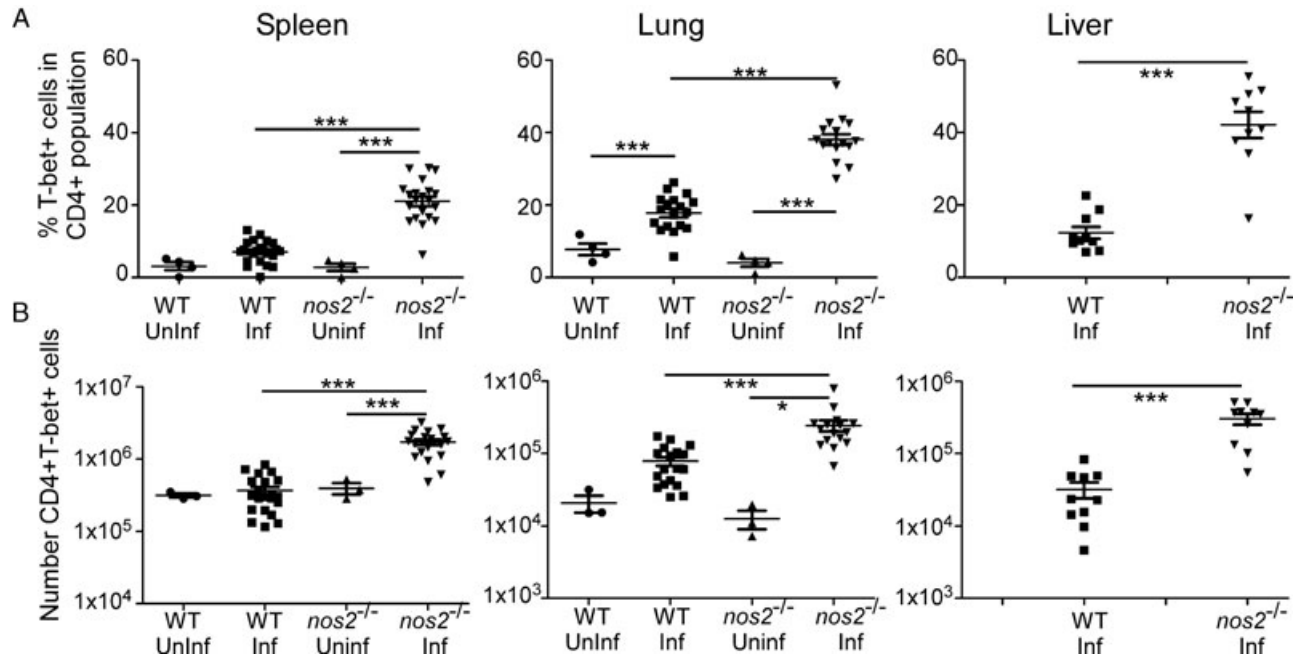

Figure 3. The number of $CD4^+$ T-bet^+ T cells is increased in the organs of *Mycobacterium avium* infected *nos2*$^{-/-}$ mice. WT (WT) and *nos2*$^{-/-}$ mice were either left uninfected (Uninf) or infected (Inf) intravenously with 10^6 *M. avium* 25291 and spleen, lungs, and livers harvested from day 60 through day 120. The organs were processed for flow cytometry and the (A) frequency and (B) number of $CD4^+$T-bet^+ cells within the organs determined. Each symbol represents an individual sample and data are shown as mean ± SEM of $n = 4$–22, pooled from the five (spleen), four (lung), or two (liver) experiments performed. $^*p < 0.05$, $^{**}p < 0.01$, $^{***}p < 0.001$, ANOVA.

nitric oxide in induction of IL-4 and reduction of VLA-4 in the $CD4^+CD44^{hi}CD69^{lo}$ population may reflect a novel regulatory mechanism for the action of nitric oxide on Th1 effector function.

Nitric oxide inhibition restricts accumulation of $CD69^{lo}$T-bet^+ $CD4^+$ T cells and expression of VLA-4

To confirm that nitric oxide was the active agent limiting the specific subset of activated $CD4^+$ T cells in *M. avium* infected mice, we delivered a specific inhibitor of nitric oxide synthase activity to infected mice and monitored the development of specific T-cell subsets. In these experiments, we treated mice early in infection, as we wanted to be able to detect the $CD69^{lo}$T-bet^+ $CD4^+$ T-cell population in the WT mice. Mice were infected and either left untreated or treated with aminoguanidine [36] from day 0 to day 30 or day 20 to day 30 and the phenotype of the activated $CD4^+$ T-cell population in the infected organs determined by flow cytometry. We found that both $CD69^{hi}$T-bet^+ and $CD69^{lo}$T-bet^+ $CD4^+$ T cells could be detected in the organs of untreated infected mice (Fig. 6A) and that the frequency of $CD69^{hi}$T-bet^+ $CD4^+$ T cells was either unaffected (spleen) or modestly reduced by aminoguanidine treatment (lung and liver) (Fig. 6A, top panels). In contrast, the frequency of $CD69^{lo}$T-bet^{hi} $CD4^+$ T cells significantly increased in the organs of all treated mice (Fig. 6A, lower panels). These data indicate that the presence of nitric oxide influences the expression of CD69 in activated $CD4^+$ T cells in all infected organs.

Based on the array data (Fig. 5B), we also wanted to determine the impact of nitric oxide on the expression of the VLA-4 marker in $CD4^+$ T cells by measuring the expression of the inducible subunit CD49d in the infected and aminoguanidine-treated mice. Using flow cytometry, we found that infection resulted in increased expression of VLA-4 on T-bet^+ $CD4^+$ T cells and that inhibition of nitric oxide generation resulted in further increased expression of this marker (Fig. 6B, upper panels). There was also an increased frequency of VLA-4^+Tbet^+ cells in the aminoguanidine-treated mice (Fig. 6B, bottom panels). These data demonstrate that nitric oxide limits the expression of VLA-4 on the activated $CD4^+$ T cells in mycobacterially infected mice.

Discussion

In the low dose model of infection, *M. avium* strain 25291 generates highly necrotic lesions resembling those induced by *M. tuberculosis* in humans and the development of necrosis is entirely dependent upon IFN-γ, IL-12p40, and $CD4^+$ T cells [32, 37]. In high-dose infection models, this strain of *M. avium* results in loss of $CD4^+$ T cells [38] and phagocyte-dominated lesions that do not become necrotic [32]. We wanted to determine whether the impact of nitric oxide on the granulomatous response to *M. avium* 25291 was related to the impact of nitric oxide on $CD4^+$ Th1 cells. The data show that in the absence of Nos2, the inflammatory site in the liver of *M. avium* 25291 infected mice is indeed altered. The WT lesion is characterized by the accumulation of F4/80^+,

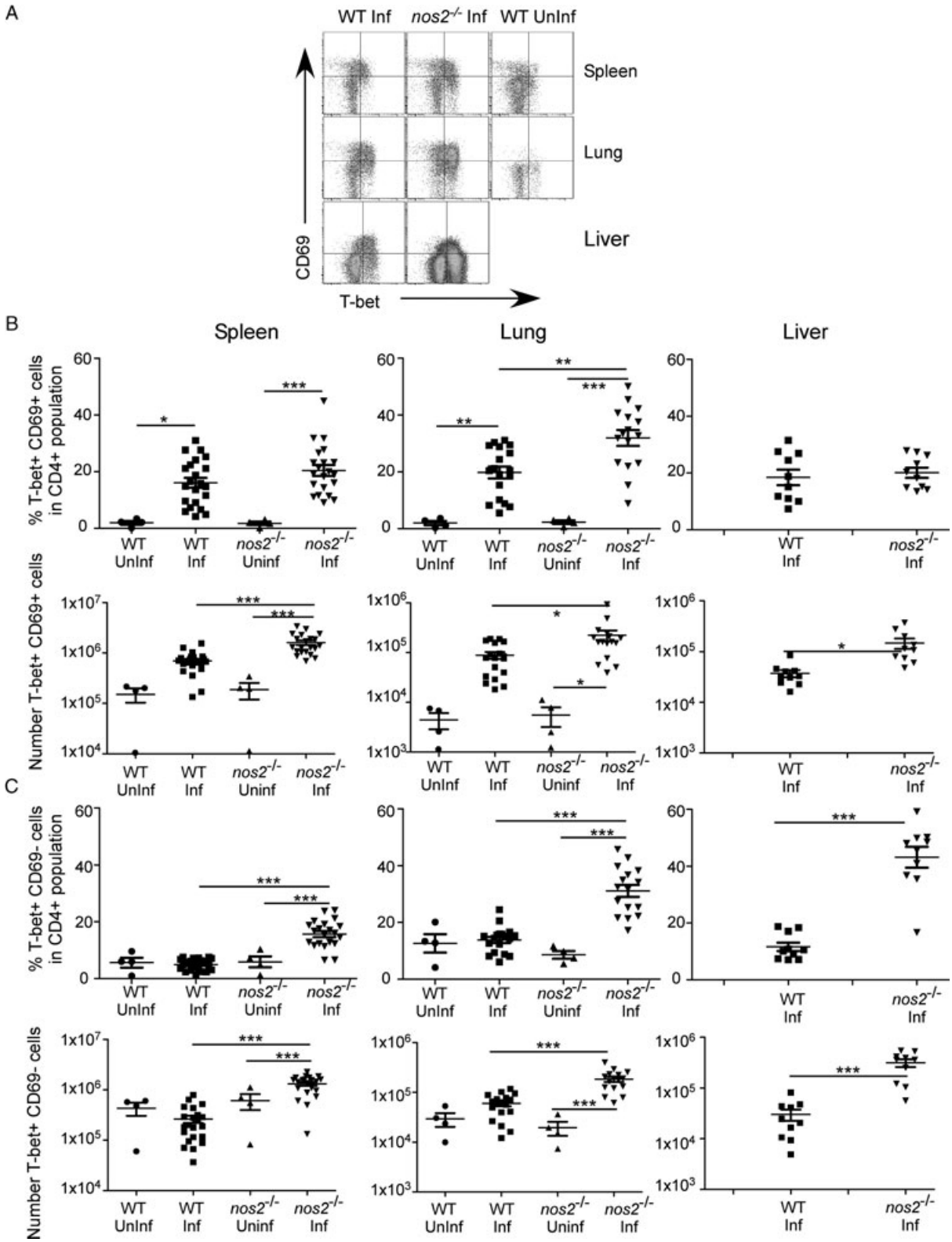

Figure 4. A subset of CD4$^+$T-bet$^+$ cells accumulates in the absence of *nos2*. WT (WT) and *nos2*$^{-/-}$ mice were either left uninfected (Uninf) or infected (Inf) intravenously with 10^6 *Mycobacterium avium* 25291 and spleen, lungs, and livers harvested from day 60 through day 120. (A) Live lymphocytes were gated using doublet discrimination, CD3$^+$, and CD4$^+$ expression (Supporting Information Fig. 2A) and then analyzed for T-bet and CD69 expression. The frequency and number of (B) CD4$^+$T-bet$^+$CD69^{hi} and (C) CD4$^+$T-bet$^+$CD69^{lo} were calculated. Each symbol represents an individual sample and data are shown as mean ± SEM of $n = 4$–22, pooled from the five (spleen), four (lung), or two (liver) experiments performed. $^*p < 0.05$, $^{**}p < 0.01$, $^{***}p < 0.001$; ANOVA.

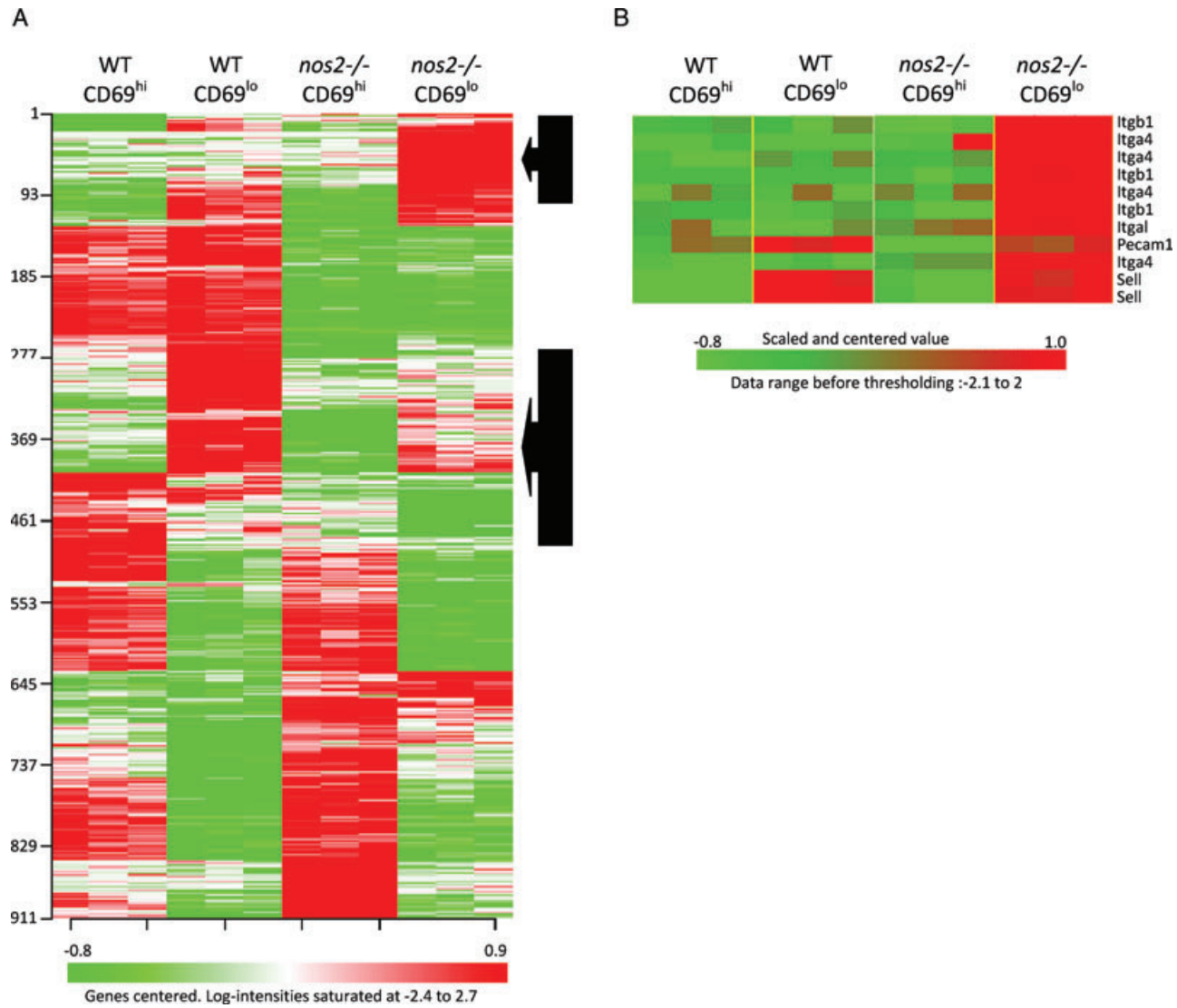

Figure 5. $CD4^+CD44^{hi}$T-bet^+CD69^{hi} and $CD4^+CD44^{hi}$T-bet^+CD69^{lo} cells represent populations with distinct transcriptomes in vivo. WT and $nos2^{-/-}$ mice were infected intravenously with 10^6 *Mycobacterium avium* 25291, spleens were harvested on day 80, and the $CD4^+CD44^{hi}CD69^{hi}$ and $CD4^+CD44^{hi}CD69^{lo}$ populations separated by FACS (Supporting Information Fig. 2B). mRNA extracted from the sorted cells underwent microarray analysis to define differential gene expression between the populations as well as between WT and $nos2^{-/-}$ mice (i.e. four distinct classes). (A) Differential gene expression between the WT and $nos2^{-/-}$ genotypes and the $CD69^{hi}$ and $CD69^{lo}$ populations (i.e. four classes). Array data were centered and normalized whereupon gene expression values were filtered to exclude genes with less than 1.5 differential expression (F-test using a *p*-value threshold of 0.005). Genes were clustered based on patterns of expression without bias. (Arrows mark gene expression clusters that differ between WT and $nos2^{-/-}$ $CD4^+CD44^{hi}CD69^{lo}$ populations.) (B) Biological pathway analysis was performed on the four classes of array data by screening 3079 filtered unique probes against 218 predefined gene lists (BioCarta Pathways). The "Adhesion Molecule Expression on Lymphocytes" pathway was over-represented in the data set compared with that from random chance ($p = 0.00031$, LS Permutation test). Multiple probes targeted the same gene resulting in three replicates of *Itgb1* and four replicates of *Itga4*.

$p22\text{-}phox^+$ monocytic phagocytes. In contrast, the absence of Nos2 resulted in increased cellular diversity in the granuloma with $F4/80^+$ $p22\text{-}phox^+$ staining phagocytes associating with many more lymphocytes and neutrophils accumulating in foci within the lesions. Thus while the WT mice did not control the bacterial growth as effectively as the $nos2^{-/-}$ mice, the lesions that developed were less complex and showed no sign of incipient necrosis. In the absence of Nos2, we show that activated T cells expressing the Th1-associated T-bet transcription factor and which are low in expression of CD69 but high in expression of VLA-4, accumulated to a much higher degree within the lesions. This accumulation of activated effector T cells was associated with the formation of a complex granuloma.

The importance of the $CD4^+$ T-cell population during granuloma development and control of mycobacterial infection make understanding the regulation of this population an important goal. Previous data has shown that there is an increase in the IFN-γ response in infected $nos2^{-/-}$ mice [6] and our data complement

Table 1. Specific gene expression in $CD4^+CD44^{hi}$ populations differentially expressing CD69 isolated from the spleens of *Mycobacterium avium* infected WT and *nos2*$^{-/-}$ mice

Gene[a]	[b]WT $CD69^{lo}$ Average ± SD[c]	*p* versus *nos2*[d]	*p* versus hi	*nos2*$^{-/-}$ $CD69^{lo}$ Average ± SD	*p* versus hi	WT $CD69^{hi}$ Average ± SD	*p* versus *nos2*	*nos2*$^{-/-}$ $CD69^{hi}$ Average ± SD
il2 1449990_at	3.63 ± 0.76	ns	**	4.20 ± 0.11	**	6.38 ± 0.59	*	4.94 ± 0.11
il2ra(#) 1420691_at	4.97 ± 0.20	ns	***	4.86 ± 0.13	***	6.68 ± 0.05	ns	7.13 ± 0.31
il2rb(#) 1417546_at	7.73 ± 0.51	ns	*	8.38 ± 0.30	**	8.66 ± 0.13	**	9.50 ± 0.25
il4 1449864_at	6.58 ± 0.23	***	*	4.36 ± 0.34	*	7.26 ± 0.36	*	5.88 ± 0.65
il4ra 1421034_a_at	8.85 ± 0.17	**	ns	7.91 ± 0.19	**	8.73 ± 0.19	ns	9.07 ± 0.14
Ifng 1425947_at	12.3 ± 0.91	ns	ns	13.5 ± 0.15	**	11.8 ± 0.66	ns	12.5 ± 0.35
ifngr2 1423557_at	5.48 ± 0.55	*	ns	3.97 ± 0.47	ns	5.52 ± 0.24	***	3.87 ± 0.20
bcl2(#) 1440770_at	9.81 ± 0.36	**	**	7.73 ± 0.53	ns[e]	8.10 ± 0.06	**	6.98 ± 0.22
itgb1(#) 1426918_at	8.54 ± 0.27	**	ns	10.4 ± 0.46	**	8.70 ± 0.08	ns[e]	8.29 ± 0.26
itga4(#) 1421194_at	8.11 ± 0.1	***	ns	9.33 ± 0.07	***	8.05 ± 0.07	ns[e]	8.42 ± 0.05

[a] Gene represented by specific probes on array. Some genes (marked #) are detected by several probes, in this case, a probe result representative of all probes for that gene is shown. The probe used is listed under the gene name.
[b] RNA from FACS sorted cells of specific $CD4^+CD44^{hi}$CD69 variable phenotype from wild type (WT) and *nos2*$^{-/-}$ mice infected 80 days previously with *M. avium*
[c] The log2 expression signal for each of the individual samples within a class ($n = 3$) was measured and the average ± SD for each class is shown.
[d] The values from samples within each group were compared to the values from the other groups and the statistical difference between the means was determined by the Student's *t*-test (i.e. between genotypes WT versus *nos2*$^{-/-}$ and phenotypes $CD69^{lo}$ versus $CD69^{hi}$).
[e] For this comparison, only one or two probes showed significance and the majority showed no significance.

this by showing the increased accumulation of T-bet expressing cells in the absence of *nos2*$^{-/-}$. These T-bet expressers are likely high producers of IFN-γ [39] and their accumulation will contribute to the higher circulating level of IFN-γ in infected *nos2*$^{-/-}$ mice. It has been reported that IFN-γ and nitric oxide regulate the T-cell response in mycobacterial disease [4] but the details of this control are not fully defined. IFN-γ serves to drive T-cell apoptosis during mycobacterial infection via direct and indirect effects [26, 40] and protection against IFN-γ-induced autophagy is mediated by *lrgm1* [41]. We have previously shown that in vitro generated effector cells, regardless of antigen specificity, are susceptible to the IFN-γ-mediated detrimental effects of the conditions induced by *M. avium* strain 25291 [34]. We now show that there is a specific subset within the pool of activated T cells that is more susceptible to nitric oxide and that these T cells can be characterized by a distinct phenotypic and transcriptional profile.

The potential function of the $CD4^+CD69^{hi}$ and $CD4^+CD69^{lo}$ populations in the mycobacterial granuloma is addressed by the data presented here. In particular, the IL-2 data suggest that the $CD4^+CD44^{hi}CD69^{hi}$ cells are more likely to be able to proliferate and that the $CD4^+CD44^{hi}CD69^{lo}$ cells are more akin to the highly differentiated cells seen in the tuberculosis model [31].

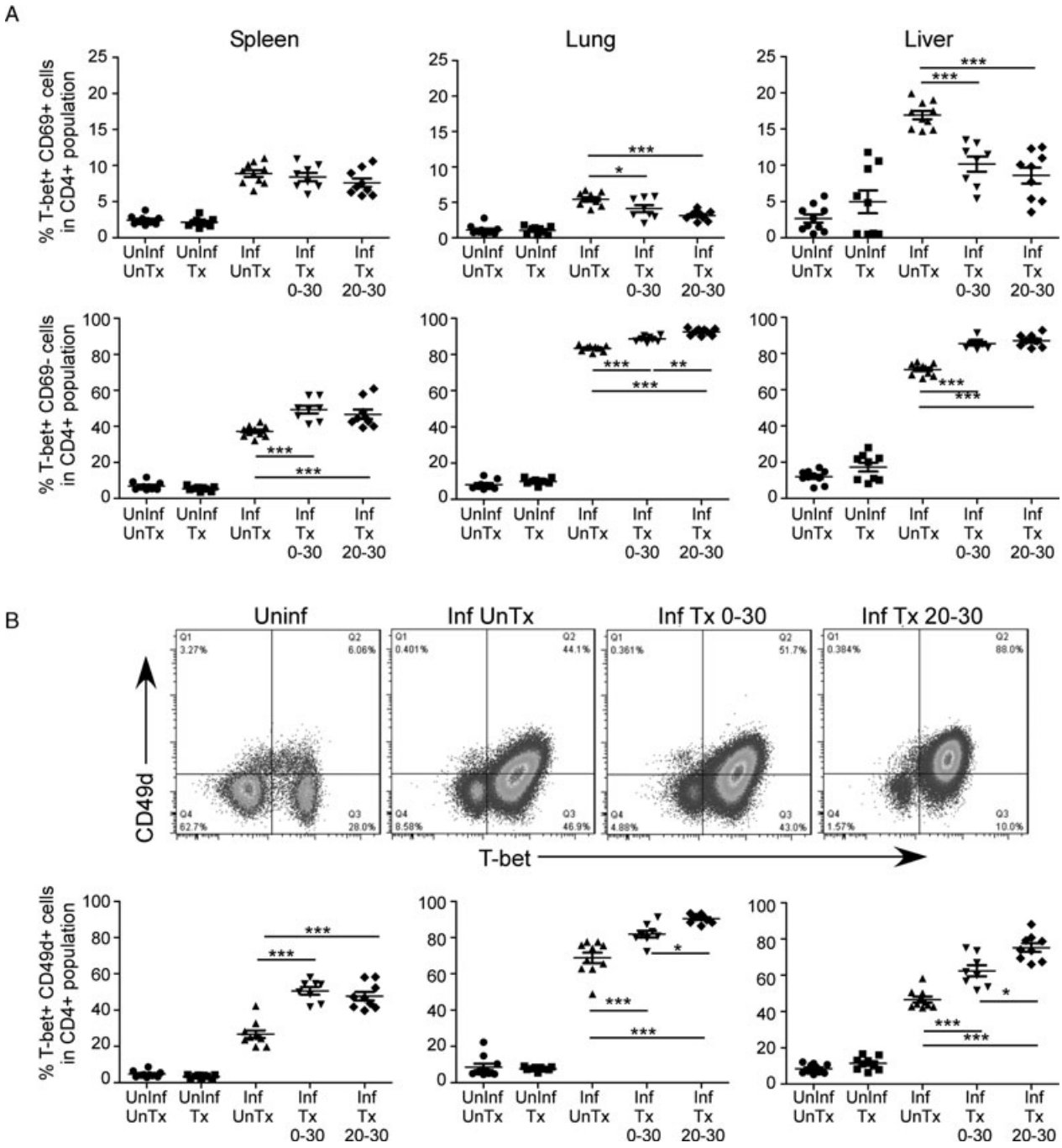

Figure 6. Nitric oxide inhibition results in increased accumulation of $CD4^+T\text{-}bet^+CD69^{lo}$ cells and increased expression of VLA-4 on $T\text{-}bet^+$ $CD4^+$ T cells. WT mice were either left uninfected (UnInf) or infected (Inf) intravenously with 10^6 *M. avium* 25291 and either left untreated (UnTx) or treated (Tx) with the Nos2 inhibitor aminoguanidine throughout the infection (0–30), or for the last 10 (20–30) days of the infection. (A) Spleens, livers, and lungs were harvested on day 30, the organs processed for flow cytometry and the frequency of $T\text{-}bet^+CD69^{hi}$ (top) and $T\text{-}bet^+CD69^{lo}$ (bottom) in the $CD4^+$ population determined. (B) The expression of T-bet and CD49d were also assessed and the frequency of $T\text{-}bet^+CD49d^+$ cells within the $CD4^+$ population in the organs of infected and treated WT mice determined. Data points are for individual mice, data are shown as mean ± SEM of $n = 10$, and are pooled from two experiments. $^*p < 0.05$, $^{**}p < 0.01$, $^{***}p < 0.001$, ANOVA.

Similarly, higher expression of the apoptosis-related *bcl2* [42] in the WT populations compared with the *nos2*$^{-/-}$-derived populations suggests that nitric oxide does promote apoptosis in these effector cells. Most intriguing, however, is the strong difference seen in the $CD4^+CD44^{hi}CD69^{lo}$ population with regard to VLA-4 and IL-4 in the absence of nitric oxide. IL-4 has been shown to limit VLA-4 expression on activated $CD4^+$ T cells and this reduces migration of cells into lesional sites [43–45]. Further, upregulation

of VLA also increases pathogenicity of T cells [46] and improves SLP-76 interaction with ZAP-70 within the immunological synapse [47]. Thus, it is possible that in the absence of nitric oxide, the $CD4^+CD44^{hi}CD69^{lo}$ cells produce less IL-4 and it is this that allows the observed greater VLA-4 expression. The published data also support the hypothesis that increased VLA-4 will allow for improved in vivo function and improved ability to accumulate within the granuloma.

One could propose therefore that the level of nitric oxide within the lesional site can dramatically impact the local protective and immunopathological response by reducing accumulation of specific subsets of activated effector cells and by altering the potency of the lymphocytes with regard to accumulation within the lesion and cytokine production. By demonstrating the differential impact of nitric oxide on distinct functional subsets of cells, we have identified a mechanism whereby protection and pathology in mycobacterial disease are modulated by nitric oxide.

Conclusion

The development of inflammation during mycobacterial infection is an important component of the disease process and is actively modulated by $CD4^+$ T cells. Herein, we demonstrate that within the pool of effector T cells, there is an activated T-cell subset that is more susceptible to the regulatory factors active within the granuloma. Defining the relative protective and pathological role of this activated T-cell subset ($CD4^+$T-bet$^+CD69^{lo}VLA4^{hi}$) will allow for improved vaccination and immunotherapeutic intervention.

Materials and methods

Mice

All mice were bred at the Trudeau Institute and were treated according to National Institutes of Health and Trudeau Institute Animal Care and Use Committee guidelines. All animal protocols used herein were approved by the Trudeau Institute Animal Care and Use Committee. C57BL/6 and B6.129P2-*nos2*^{tm1Lau} (*nos2*$^{-/-}$) (originally purchased from JAX Mice, Maine) were used in these experiments.

Experimental infection and enumeration of viable bacteria

Mice were infected with *M. avium* 25291 (ATTC) at a dose of 1×10^6 cfu by lateral tail vein injection. The level of bacteria in specific organs was determined by homogenizing the organs and plating on agar and counting colonies [48,49]. Some infected WT mice were treated with aminoguanidine hemisulfate (Sigma-Aldrich) at 2.5 g/100 mL in the drinking water for defined periods of time; control mice received water without drug.

Histology

Liver sections were placed in 10% neutral-buffered formalin, blocked in paraffin, processed for light microscopy, and stained with hematoxylin and eosin to provide cell structure. For immunofluorescence staining, liver sections were harvested into cold HBSS and 3–4 mm sections cut with a scalpel. Sections were placed in 4% low-melt agarose (Lonza Seaplaque Agarose, Fisher Scientific) in HBSS. The solidified gel containing sections of liver was then sectioned using a vibrating microtome cooled to 4°C (Leica VT1000) and 200-micron sections were collected into 12-well plates containing HBSS, FcBlock, 5% normal mouse serum. Sections were stained with fluorescently labeled antibodies, anti-CD4 PE (RM4–5), anti-CD8 PE (clone 53–6.7), Ly6G PE (clone 1A8) (all from BD Biosciences, CA, USA) and F4/80 Alexa647 (clone Cl:A3–1, AbD Serotec, NC, USA) were added to the well at a dilution of 1:200 except for F4/80 which was used at 1:75. Tissues were incubated for 2 h on ice and then washed twice with excess PBS for 15 min each. Cryosections were generated from liver tissue harvested in Tissue-Tek which were then air dried, fixed with neutral-buffered formalin, blocked with 10% normal mouse serum/1% Triton X-100/1% Tween-20 and exposed to the following fluorescently labeled antibodies–CD8 allophycocyanin (clone 53–6.7, eBioscience, CA, USA), CD4 PE (as above), polyclonal rabbit anti-p22-phox (Santa Cruz Biotechnology, CA, USA), polyclonal Rabbit anti-iNOS (BD Transduction Laboratories, CA, USA) and anti-Rabbit 488 (Invitrogen, NY, USA). Sections were also exposed to Hoechst DNA stain. All sections were exposed to appropriate laser light using the Leica SP5 confocal (Leica Microsystems, Germany) and the light emissions detected using photomultiplier tubes (PMTs) of the appropriate bandwidth. Emission spectra were collected using sequential scanning to avoid spectral bleed-through. The data were collected as Leica image files using LAS-AF version 2.2.1 software (Leica) and converted into TIFF using Fiji software (http://fiji.sc/wiki/index.php/Fiji). Sections were incubated with either CD4/CD8 and F4/80 antibodies or Ly6G and F4/80 antibodies.

Cell preparation and flow cytometry and cell sorting

Lungs of experimental mice were perfused with cold saline containing heparin and placed in cold DMEM (Mediatech-Cellgro). Livers and spleens were taken directly from experimental mice and placed in cold DMEM. All organs were then sectioned using fresh sterile razor blades and placed in DMEM containing collagenase IX (0.7 mg/mL; Sigma-Aldrich) and DNase (30 μg/mL; Sigma-Aldrich) at 37°C for 30 min [49,50]. Digested tissue was gently dispersed by passage through a 70 μm pore size nylon tissue strainer (Falcon; BD Biosciences); the resultant single-cell suspension was treated with Gey's solution to remove

any residual RBC, washed twice, and counted. The liver cells were further processed over a 40%:80% Percoll (GE Healthcare) gradient and then washed and counted. Cell suspensions were stained for surface markers, washed, processed for intracellular staining using the eBioscience "Transcription factor staining buffer set" (eBioscience) according to the manufacturer's instructions and then stained for T-bet. The antibodies were titrated for use and consisted of anti-CD3 (Clone 17A2) labeled with eFluor450, anti-CD4 (clone RM4–5) labeled with PerCP-Cy5.5, anti-CD69 (clone H1.2F3) labeled with PE-Cy7, anti-CD44 (clone IM7) labeled with allophycocyanin-eFluor780, and anti-T-bet (clone 4B10) labeled with PE (all from eBioscience). Data from stained cells were collected using Diva software on an LSRII flow cytometer (BD Biosciences) and analyzed using FlowJo software (Tristar) and the gating system is shown in Supporting Information Fig. 2A. Cells stained as above were also sorted to purity on a BD Influx, 11 color, four laser system based on live lymphocyte, CD4 positive, CD44 high, and then separated based on the expression of CD69. An example of the purity of the sorted populations is shown in Supporting Information Fig. 2B.

Preparation of nucleic acid and microarray analysis

RNA was extracted from purified populations and DNA removed with the RNeasy Plus Mini Kit (Qiagen, CA, USA) according to the manufacturer's instructions. RNA was quality tested and the yield was between 3.4 and 98 ng/uL per sample. The isolated RNA was used to generate cRNA which was then biotinylated and prepared according to the Affymetrix GeneChip 3′ IVT Express Protocol from 150 ng of total RNA. Following fragmentation, 10 μg of cRNA was hybridized for 16 h at 45°C on Mouse Genome 430 2.0 arrays. Arrays were washed and stained in the Affymetrix Fluidics Stations 450. The arrays were scanned using an Affymetrix GeneChip Scanner 3000 7G. Initial QC was performed with Affymetrix Expression Console using the RMA algorithm with quantile normalization and general background correction.

BRB-Arraytools was used for statistical analysis and results visualization [51] as described [52, 53]. Preprocessing with robust multi-array average with GC-content background correction was performed on all CEL files to provide background correction using probe sequence and GC content, quantile normalization, and a robust multichip model fit using median polish [54] (Supporting Information Table 1). GC-content background correction was selected from various other background correction algorithms because it yielded the minimum intraclass variation for a subset of experimentally relevant genes [55]. Spot filters, normalization, gene filters, and gene subsets: No spot filtering was applied. Log2 normalization was applied. The median array was used as a reference array. The default gene filters were applied which excluded genes having less than 20% of their expression values and having at least a 1.5-fold change from the median expression value or if greater than 50% of the expression values are missing. Only named genes, that is, those without "NA" as their annotated gene identifier were analyzed, thus excluding nonspecific probes and array-specific controls. Following these processes, 3366 specific probes were identified as differentially expressed with 3079 named genes identified. Gene annotation: Genes were annotated using the Affymetrix HT_MG-430B Array (mouse4302) in BRB-Arraytools. Class comparison: Class comparison was then used to identify specific genes whose expression correlated with the experimental group (i.e. WT $CD69^{lo}$, WT $CD69^{hi}$, $nos2^{-/-}CD69^{lo}$ or $nos2^{-/-}CD69^{hi}$) using a univariate F-test at a significance threshold of $p = 0.001$ that yielded 911 genes.

Gene set class comparison was used to identify biologically relevant pathways by comparing the set of experimentally identified differentially expressed genes with 218 predefined BioCarta pathway gene lists (biocarta.com) representing previously investigated biological pathways. Gene set class comparison identifies biological pathways that are over-represented in the experimental data by comparing the number of differentially expressed genes for a given BioCarta pathway with that expected by random chance alone. The significance threshold for this test was $p = 0.005$ using a univariate F-test to define differentially expressed genes (as above) with an LS permutation test used to identify BioCarta gene sets having more genes differentially expressed among the phenotype classes than expected by chance. Of the 218 BioCarta gene lists tested, 107 gene lists contained one or more differentially expressed genes, and of these BioCarta gene lists, two were identified as significantly enriched for differentially expressed genes: "Adhesion Molecules on Lymphocytes" and "Monocyte and its Surface Molecules," containing 11 and 12 genes, respectively. When examined, these two gene sets contained 11 of 12 identical genes.

Hierarchical clustering of genes was used to survey the differentially expressed genes to identify global patterns of expression. To perform this analysis, the genes were centered and scaled, using one-minus correlation with average linkage computed.

Statistics

Differences between the means of experimental groups were analyzed using the two-tailed Student's *t*-test or ANOVA as appropriate. Differences were considered significant where $p \leq 0.05$. Inherently logarithmic data from bacterial growth were transformed for statistical analysis.

Acknowledgements: This work was supported by the Trudeau Institute, Inc., NIH grants AI46530 and AI069121 and an American Lung Association DeSouza Award to AMC.; PTDC/SAU-MII/099102/2008 from the FCT (Fundação para a Ciência e a Tecnologia) to RA. The Authors would like to thank Flow Cytometry Core and the Imaging Core at Trudeau Institute and Phyllis Spatrick at the Genomic Core Facility at UMASS Medical School for excellent technical support.

Conflict of interest: The authors declare no financial or commercial conflict of interest.

References

1 **Cooper, A. M.**, Cell mediated immune responses in tuberculosis. *Annu. Rev. Immunol.* 2009. **27**: 393–422.

2 **Nathan, C.**, Inducible nitric oxide synthase: what difference does it make? *J. Clin. Invest.* 1997. **100**: 2417–2423.

3 **Bogdan, C.**, Nitric oxide and the immune response. *Nat. Immunol.* 2001. **2**: 907–916.

4 **Cooper, A. M., Adams, L. B., Dalton, D. K., Appelberg, R. and Ehlers, S.**, IFN-γ and NO in mycobacterial disease: new jobs for old hands. *Trends Microbiol.* 2002. **10**: 221–226.

5 **Niedbala, W., Cai, B. and Liew, F. Y.**, Role of nitric oxide in the regulation of T-cell functions. *Ann. Rheum. Dis.* 2006. **65**: iii37–iii40.

6 **Gomes, M. S., Florido, M., Pais, T. F. and Appelberg, R.**, Improved clearance of *Mycobacterium avium* upon disruption of the inducible nitric oxide synthase gene. *J. Immunol.* 1999. **162**: 6734–6739.

7 **Hirst, D. and Robson, T.**, Nitric oxide and physiology. In **McCarthy, H. O. and Coulter, J. A.** (Eds.), *Methods in Molecular Biology* Springer, London, 2011, pp. 1–13.

8 **Xu, W., Charles, I. G. and Moncada, S.**, Nitric oxide: orchestrating hypoxia regulation through mitochondrial respiration and the endoplasmic reticulum stress response. *Cell. Res.* 2005. **15**: 63–65.

9 **Hirst, D. and Robson, T.**, Nitrosative stress in cancer therapy. *Front. Biosci.* 2007. **12**: 3406–3418.

10 **Brown, G.**, Regulation of mitochondrial respiration by nitric oxide inhibition of cytochrome c oxidase. *Biocim. Biophys. Acta – Bioenerg.* 2001. **1504**: 46–57.

11 **Gupta, M. P., Ober, M. D., Patterson, C., Al-Hassani, M., Natarajan, V. and Hart, C. M.**, Nitric oxide attenuates H_2O_2-induced endothelial barrier dysfunction: mechanisms of protection. *Am. J. Physiol. – Lung Cell. Mol. Physiol.* 2001. **280**: L116–L126.

12 **Szabo, C., Ischiropoulos, H. and Radi, R.**, Peroxynitrite: biochemistry, pathophysiology and development of therapeutics. *Nat. Rev. Drug Discov.* 2007. **6**: 662–680.

13 **Bogdan, C.**, Regulation of lymphocytes by nitric oxide. *Methods Mol. Biol.* 2011. **677**: 375–393.

14 **Fischer, T. A., Palmetshofer, A., Gambaryan, S., Butt, E., Jassoy, C., Walter, U., Sopper, S. et al.,** Activation of cGMP-dependent protein kinase Iβ inhibits interleukin 2 release and proliferation of T-cell receptor-stimulated human peripheral T cells. *J. Biol. Chem.* 2001. **276**: 5967–5974.

15 **Millar, A. E., Sternberg, J., McSharry, C., Wei, X.-Q., Liew, F. Y. and Turner, C. M. R.**, T-cell responses during *Trypanosoma brucei* infections in mice deficient in inducible nitric oxide synthase. *Infect. Immun.* 1999. **67**: 3334–3338.

16 **Albina, J., Abate, J. and Henry, W.**, Nitric oxide production is required for murine resident peritoneal macrophages to suppress mitogen-stimulated T-cell proliferation. Role of IFN-gamma in the induction of the nitric oxide-synthesizing pathway. *J. Immunol.* 1991. **147**: 144–148.

17 **Gregory, S., Wing, E., Hoffman, R. and Simmons, R.**, Reactive nitrogen intermediates suppress the primary immunologic response to Listeria. *J. Immunol.* 1993. **150**: 2901–2909.

18 **Laroux, F., Lefer, D., Kawachi, S., Scalia, R., Cockrell, A., Gray, L., Van der Heyde, H. et al.,** Role of nitric oxide in the regulation of acute and chronic inflammation. *Antioxid. Redox Signal.* 2000. **2**: 391–396.

19 **Niedbala, W., Cai, B., Liu, H., Pitman, N., Chang, L. and Liew, F. Y.**, Nitric oxide induces CD4+CD25 +Foxp3− regulatory T cells from CD4+CD25− T cells via p53, IL-2, and OX40. *Proc. Natl. Acad. Sci. USA* 2007. **104**: 15478–15483.

20 **Niedbala, W., Alves-Filho, J. C., Fukada, S. Y., Vieira, S. M., Mitani, A., Sonego, F., Mirchandani, A. et al,** Regulation of type 17 helper T-cell function by nitric oxide during inflammation. *Proc. Natl. Acad. Sci. USA* 2011. **108**: 9220–9225.

21 **Diefenbach, A., Schindler, H., Röllinghoff, M., Yokoyama, W. and Bogdan, C.**, Requirement for type 2 NO synthase for IL-12 signaling in innate immunity. *Science* 1999. **284**: 951–955.

22 **Huang, F.-P., Niedbala, W., Wei, X.-Q., Xu, D., Feng, G.-j., Robinson, J. H., Lam, C. et al.,** Nitric oxide regulates Th1 cell development through the inhibition of IL-12 synthesis by macrophages. *Eur. J. Immunol.* 1998. **28**: 4062–4070.

23 **Niedbala, W., Wei, X.-Q., Campbell, C., Thomson, D., Komai-Koma, M. and Liew, F. Y.**, Nitric oxide preferentially induces type 1 T-cell differentiation by selectively up-regulating IL-12 receptor β2 expression via cGMP. *Proc. Natl. Acad. Sci. USA* 2002. **99**: 16186–16191.

24 **Niedbala, W., Wei, X.-Q., Piedrafita, D., Xu, D. and Liew, F. Y.**, Effects of nitric oxide on the induction and differentiation of Th1 cells. *Eur. J. Immunol.* 1999. **29**: 2498–2505.

25 **Lee, S.-W., Choi, H., Eun, S.-Y., Fukuyama, S. and Croft, M.**, Nitric oxide modulates TGF-β–directive signals to suppress Foxp3+ regulatory T-cell differentiation and potentiate Th1 development. *J. Immunol.* 2011. **186**: 6972–6980.

26 **Dalton, D. K., Haynes, L., Chu, C. Q., Swain, S. L. and Wittmer, S.**, Interferon gamma eliminates responding CD4 T cells during mycobacterial infection by inducing apoptosis of activated CD4 T cells. *J. Exp. Med.* 2000. **192**: 117–122.

27 **Nabeshima, S., Nomoto, M., Matsuzaki, G., Kishihara, K., Taniguchi, H., Yoshida, S. and Nomoto, K.**, T-cell hyporesponsiveness induced by activated macrophages through nitric oxide production in mice infected with *Mycobacterium tuberculosis*. *Infect. Immun.* 1999. **67**: 3221–3226.

28 **MacMicking, J. D., North, R. J., LaCourse, R., Mudgett, J., Shah, S. K. and Nathan, C. F.**, Identification of NOS2 as a protective locus against tuberculosis. *Proc. Natl. Acad. Sci. USA* 1997. **94**: 5243–5248.

29 **Lousada, S., Flórido, M. and Appelberg, R.**, Regulation of granuloma fibrosis by nitric oxide during *Mycobacterium avium* experimental infection. *Int. J. Exp. Pathol.* 2006. **87**: 307–315.

30 **Ehlers, S., Kutsch, S., Benini, J., Cooper, A. M., Hahn, C., Gerdes, J., Orme, I. M. et al.,** NOS2-derived nitric oxide regulates the size, quantity and quality of granuloma formation in *Mycobacterium avium* infected mice without affecting bacterial loads. *Immunology* 1999. **98**: 313–323.

31 **Reiley, W. W., Shafiani, S., Wittmer, S. T., Tucker-Heard, G., Moon, J. J., Jenkins, M. K., Urdahl, K. B. et al.,** Distinct functions of antigen-specific CD4 T cells during murine *Mycobacterium tuberculosis* infection. *Proc. Natl. Acad. Sci. USA* 2010. **107**: 19408–19413.

32 **Florido, M., Cooper, A. M. and Appelberg, R.**, Immunological basis of the development of necrotic lesions following *Mycobacterium avium* infection. *Immunology* 2002. **106**: 590–601.

33 **Bedard, K. and Krause, K.-H.**, The NOX family of ROS-generating NADPH oxidases: physiology and pathophysiology. *Physiol. Rev.* 2007. **87**: 245–313.

34 **Florido, M., Pearl, J., Solache, A., Borges, M., Haynes, L., Cooper, A. and Appelberg, R.**, Gamma interferon-induced T-cell loss in virulent *Mycobacterium avium* infection. *Infect. Immun.* 2005. **73**: 3577–3586.

35 **Testi, R., Phillips, J. H. and Lanier, L. L.**, Leu 23 induction as an early marker of functional CD3/T cell antigen receptor triggering. *J. Immunol.* 1989. **142**: 1854–1860.

36 **Corbett, J., Tilton, R., Chang, K., Hasan, K., Ido, Y., Wang, J., Sweetland, M. et al.,** Aminoguanidine, a novel inhibitor of nitric oxide formation, prevents diabetic vascular dysfunction. *Diabetes* 1992. **41**: 552–556.

37 **Ehlers, S., Benini, J., Held, H.-D., Roeck, C., Alber, G. and Uhlig, S.**, αβ T-cell receptor-positive cells and interferon-γ, but not inducible nitric oxide synthase, are critical for granuloma necrosis in a mouse model of mycobacteria-induced pulmonary immunopathology. *J. Exp. Med.* 2001. **194**: 1847–1859.

38 **Florido, M., Goncalves, A.-S., Silva, R. A., Ehlers, S., Cooper, A. M. and Appelberg, R.**, Resistance of virulent *Mycobacterium avium* to gamma interferon-mediated antimicrobial activity suggests additional signals for induction of mycobacteriostasis. *Infect. Immun.* 1999. **67**: 3610–3618.

39 **Mayer, K., Mohrs, K., Crowe, S., Johnson, L., Rhyne, P., Woodland, D. and Mohrs, M.**, The functional heterogeneity of type I effector T cells in response to infection is related to the potential for IFN-γ production. *J. Immunol.* 2005. **180:** 7732–7739.

40 **Li, X., McKinstry, K., Swain, S. and Dalton, D.**, IFN-gamma acts directly on activated CD4+ T cells during mycobacterial infection to promote apoptosis by inducing components of the intracellular apoptosis machinery and by inducing extracellular proapoptotic signals. *J. Immunol.* 2007. **179**: 939–949.

41 **Feng, C., Zheng, L., Jankovic, D., Báfica, A., Cannons, J., Watford, W., Chaussabel, D. et al.,** The immunity-related GTPase Irgm1 promotes the expansion of activated CD4+ T-cell populations by preventing interferon-gamma-induced cell death. *Nat. Immunol.* 2008. **9**: 1279–1287.

42 **Paoluzzi, L. and O'Connor, O.**, Targeting survival pathways in lymphoma. *Adv. Exp. Med. Biol.* 2010. **687**: 79–96.

43 **Sasaki, K., Pardee, A. D., Okada, H. and Storkus, W. J.**, IL-4 inhibits VLA-4 expression on Tc1 cells resulting in poor tumor infiltration and reduced therapy benefit. *Eur. J. Immunol.* 2008. **38**: 2865–2873.

44 **Sasaki, K., Pardee, A., Qu, Y., Zhao, X., Ueda, R., Kohanbash, G., Bailey, L. et al.,** IL-4 suppresses very late antigen-4 expression which is required for therapeutic Th1 T-cell trafficking into tumors. *J. Immunother.* 2009. **32**: 793–802.

45 **Calderon, B., Carrero, J. A., Miller, M. J. and Unanue, E. R.**, Entry of diabetogenic T cells into islets induces changes that lead to amplification of the cellular response. *Proc. Natl. Acad. Sci. USA* 2011. **108**: 1567–1572.

46 **Suvas, S., Kim, B. and Rouse, B. T.**, Homeostatic expansion of CD4+ T cells upregulates VLA-4 and exacerbates HSV-induced corneal immunopathology. *Microbes Infect.* 2008. **10**: 1192–1200.

47 **Nguyen, K., Sylvain, N. R. and Bunnell, S. C.**, T-cell costimulation via the integrin VLA-4 inhibits the actin-dependent centralization of signaling microclusters containing the adaptor SLP-76. *Immunity* 2008. **28**: 810–821.

48 **Orme, I. and Roberts, A.**, Animal models of mycobacteria infection (section 19.5.1). *Curr. Protoc. Immunol.* 2001. **30**:19.5.1–19.5.22.

49 **Roberts, A., Cooper, A., Belisle, J., Turner, J., Gonzalez-Juarerro, M. and Orme, I.**, Murine models of tuberculosis. In **Kaufmann, S. and Kabelitz, D.** (Eds.), *Methods in Microbiology*, Second Edn. Academic Press, London, 2002, pp. 433–462.

50 **Khader, S., Pearl, J., Sakamoto, K., Gilmartin, L., Bell, G., Jelley-Gibbs, D., Ghilardi, N. et al.,** IL-23 compensates for the absence of IL-12p70 and is essential for the IL-17 response during tuberculosis but is dispensable for protection and antigen-specific IFN-γ responses if IL-12p70 is available. *J. Immunol.* 2005. **175**: 788–795.

51 **Simon, R., Lam, A., Li, M., Ngan, M., Menenzes, S. and Zhao, Y.**, Analysis of gene expression data using BRB-ArrayTools. *Cancer Inform.* 2007. **3**: 11–17.

52 **Simon, R., Korn, E., McShane, L., Radmacher, M., Wright, G. and Zhao, Y.**, *Design and analysis of DNA microarray investigations*. Springer Verlag, New York, 2003.

53 **Simon, R. and Lam, A.**, *BRB array tools users technical reports*. Biometric Research Branch, National Cancer Institute, Bethesda, MD, 2006.

54 **Wu, Z., Itrizarry, R., Gentleman, R., Murillo, F. and Spencer, F.**, A model based background adjustment for oligonucleotide expression arrays. *J. Am. Stat. Assoc.* 2004. **99**: 909–917.

55 **Seo, J. and Hoffman, E.**, Probe set algorithms: is there a rational best bet? *BMC Bioinform.* 2006. **7**: 395.

Abbreviation: **VLA-4**: very late antigen-4

Full correspondence: Dr. Andrea M. Cooper, Trudeau Institute Inc., Saranac Lake NY 12983, USA
Fax: +1-518-891-5126
e-mail: acooper@trudeauinstitute.org

Received: 11/10/2011
Revised: 27/6/2012
Accepted: 10/8/2012
Accepted article online: 14/8/2012

European Journal of Immunology

Supporting Information

for

DOI 10.1002/eji.201142158

John E. Pearl, Egidio Torrado, Michael Tighe, Jeffrey J. Fountain, Alejandra Solache, Tara Strutt, Susan Swain, Rui Appelberg and Andrea M. Cooper

Nitric oxide inhibits the accumulation of $CD4^{+}CD44^{hi}Tbet^{+}CD69^{lo}$ T cells in mycobacterial infection

Pearl et al Supporting Information Figure 1

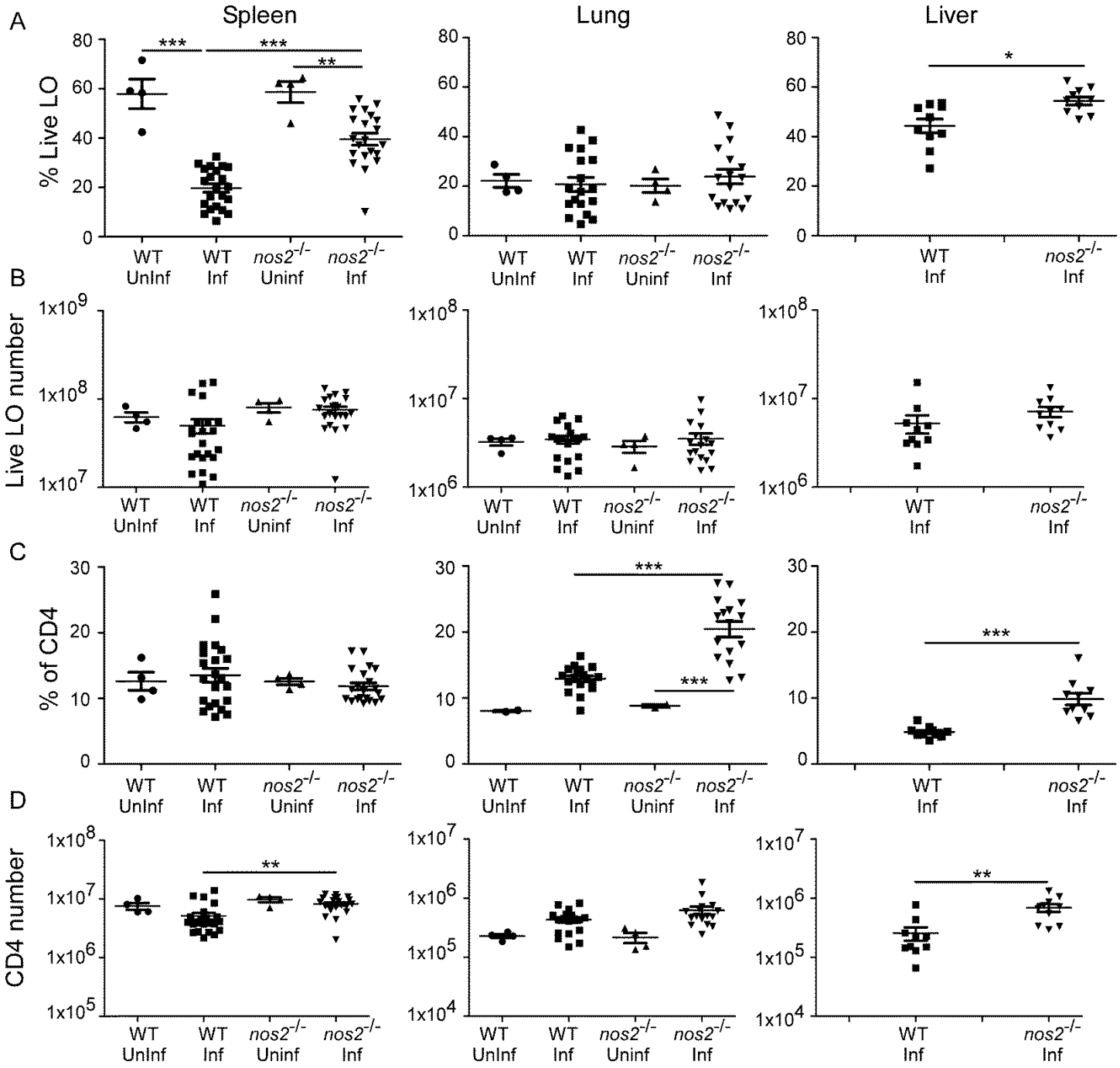

Supporting Information Figure 1. Live CD4$^+$ T-cell populations in *M. avium*-infected mice. WT and *nos2*$^{-/-}$ mice were either left uninfected (UnInf) or infected (Inf) intravenously with 10^6 *M. avium* 25291 and the spleens, lungs and livers harvested. The organs were processed for flow cytometry and the (A, C) frequency and (B, D) number of live lymphocytes (LO) (A, B) and CD4$^+$ T cells (C, D) within the organs determined. Cells were gated on live lymphocytes, doublet discrimination, and CD3$^+$, CD4$^+$ (n=4-22, *P<0.05, **P<0.01, ***P<0.001, by ANOVA).

Pearl et al Supporting Information Figure 2

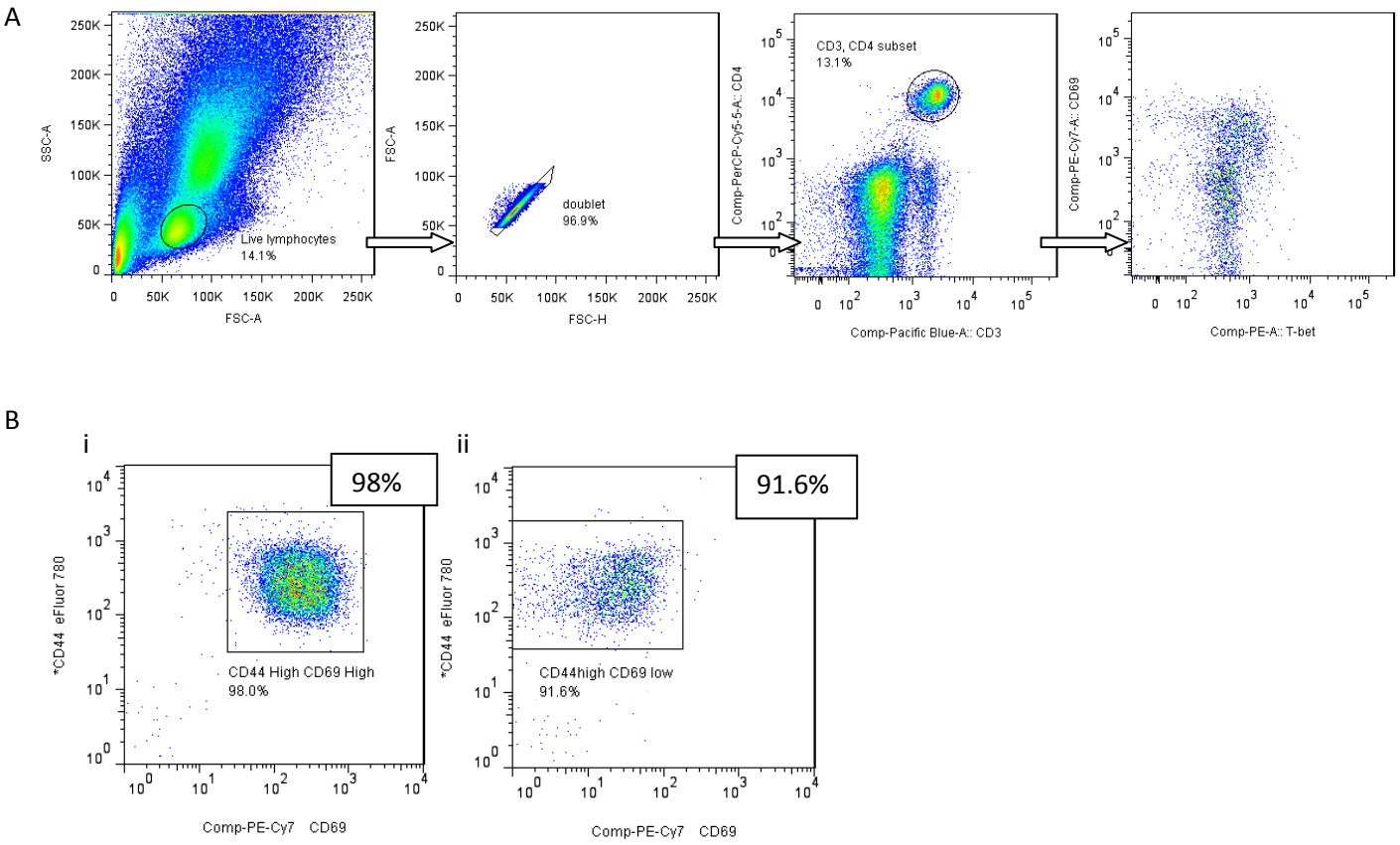

Supporting Information Figure 2. Gating scheme for flow cytometric analysis and cell sorting. (A) The gating scheme for the detection of live, single cell, $CD3^{+}CD4^{+}CD44^{+}$ T cells is shown in sequence. (B) Representative purity of the live, single cell (i) $CD4^{+}CD44^{+}CD69^{hi}$ and (ii) $CD4^{+}CD44^{+}CD69^{lo}$ cells sorted prior to RNA extraction.